Modelling Simul. Mater. Sci. Eng. **18** (2010) 085008 (13pp) doi:10.1088/0965-0393/18/8/085008

Screw dislocation mobility in BCC metals: the role of the compact core on double-kink nucleation

P A Gordon[1], T Neeraj[1], Y Li[2] and J Li[3]

[1] ExxonMobil Research and Engineering, 1545 Route 22 East, Annandale NJ, 08801, USA
[2] Zodiac Aerospace, 2239 High Hill Road, Logan NJ, 08085, USA
[3] Department of Materials Science, University of Pennsylvania 3231 Walnut St. Philadelphia PA, 19104, USA

E-mail: Peter.A.Gordon@exxonmobil.com

Received 11 June 2010, in final form 29 September 2010
Published 16 November 2010
Online at stacks.iop.org/MSMSE/18/085008

Abstract

In this work, we examine the kink-nucleation process in BCC screw dislocations using atomistic simulation and transition pathway analysis, with a particular focus on the *compact* core structure. We observe the existence of a threshold stress, which results in an abrupt change in the minimum energy path of the kink-nucleation process, and hence, a discontinuity in the activation energy versus stress for the process. The magnitude of the discontinuity is found to be related to the degree of metastability of an intermediate *split*-core structure. This feature appears to be a direct consequence of the so-called 'camel-hump' nature of the Peierls potential, which manifests itself in the existence of a metastable, intermediate split-core structure. The effect is observed in a number of empirical EAM potentials, including Fe, Ta, V, Nb and Mo, suggesting a generality to the observations.

(Some figures in this article are in colour only in the electronic version)

1. Introduction

It is well known that at low temperatures, the flow stress in α-Fe, like other body-centered cubic (BCC) metals, exhibits strong temperature dependence. This dependence arises from the motion of screw dislocations between local energetic minima (Peierls valleys), a process thought to be catalyzed through the nucleation and migration of kink pairs along the dislocation [1, 2]. As kink mobility is generally thought to be very high in metals, low temperature plasticity is thought to be controlled by the nucleation of the kink pairs.

Details of the kink-nucleation mechanism have generally been investigated with the aid of atomistic models, which have provided much insight into the nature of the dislocation core structure and the implications for mobility [3]. Early atomistic studies attributed the strong

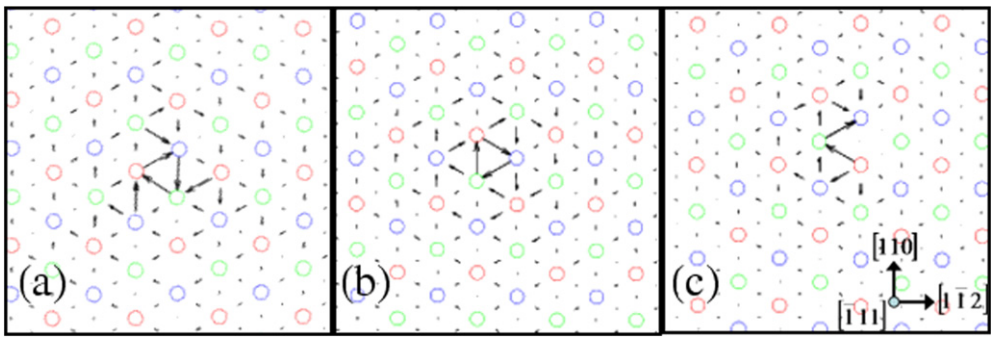

Figure 1. Differential displacement maps depicting screw dislocation structures for (*a*) degenerate core, (*b*) non-degenerate/compact core and (*c*) split core.

temperature dependence and anisotropy of plasticity to the polarized (degenerate) structure of the screw dislocation core [4], as shown in figure 1.

The implications for kink nucleation have been examined in detail for Fe potentials that predict a polarized core structure [5–7]. For instance, Wen and Ngan studied the activation pathways of kink-nucleation in Fe with an empirical potential [8] and found that the most energetically favored process predicted the correct activation energy at zero stress. However, their results significantly overestimate the flow stresses measured experimentally with increasing applied stress, suggesting that the activation volume of the nucleation process is incorrect. Such overestimation of flow stresses and the Peierls stress has plagued many previous atomistic models for α-Fe and other BCC metals [3, 9, 10]. In addition, this model predicts that motion of screw dislocations occurs, on average, along the {1 1 2} planes, even though the maximum resolved shear stress is on the {1 1 0} plane. This is in contrast to experimental observations where slip is observed to occur on {1 1 0} planes in α-Fe [1, 11].

It has been observed that atomistic potentials are capable of producing core structures significantly different than that of the non-polarized core of figure 1(*a*). Through the use of interatomic row potentials, Takeuchi [12] examined the core structure of screw dislocations in the BCC lattice and found that a polarized or non-degenerate (compact) core structure (figure 1(*b*)) could be produced depending upon the shape of the row potential. Duesbery and Vitek [13] also observed different core structures with Finnis–Sinclair type potentials [14, 15], which could be delineated based on the aspects of the shape of the {1 1 0}⟨1 1 1⟩ cross section of the γ-surface. The potentials predict a compact core structure for group VB elements (V, Nb and Ta) and polarized cores for the group VIB metals Cr, Mo and W. Finally, for α-Fe, it has been reported in the literature [16, 17] that an EAM potential for Fe due to Mendelev *et al* [18] predicted a compact core structure for the screw dislocation, in marked contrast to previously developed Fe potentials [8, 19, 20].

Interestingly, Takeuchi noted in his work that for the various interatomic row potentials studied, the compact core structure was always accompanied by a metastable *split*-core configuration (figure 1(*c*)). This correspondence has been recently confirmed again in an extensive analysis using a multi-string Frenkel–Kontorova model [21] to represent the relative slip displacement of core atoms during Peierls valley translation [22].

Application of density functional theory (DFT) methods to compute the core structure of screw dislocations in BCC metals has suggested that the compact core is the stable configuration for Ta, Mo and α-Fe [23–26]. Furthermore, differences in the gamma-surface profiles computed by DFT and by empirical potentials such as Mendelev's Fe potential have

been noted [27]. In addition, for Fe, DFT calculations have not found the presence of a metastable split-core structure [26]. This raises important questions about the influence of the compact core structure on the activation pathway and energetics for screw dislocations.

Several groups have recently employed the potential due to Mendelev to examine the dynamics of kink nucleation and glide of screw dislocations using MD simulation [16, 17]. These studies have necessarily required simulation at high applied stress and/or strain rates in order to observe motion on timescales accessible to MD. Both groups observed motion that occurs through two uncorrelated, partial kink-pair processes. We will demonstrate that more complex behavior is observed through the use of transition state theory at simulation conditions more in line with flow stress data obtained from experiment.

In this paper, we employ transition pathway analysis with the nudged elastic band (NEB) method [28–30] in conjunction with an empirical EAM potential for Fe to examine the kink-nucleation behavior at low to moderate applied stress. In particular, we find that an abrupt transition in the favored nucleation pathway exists at a stress, we term the *threshold* stress, below which the two distinct half-kink processes observed by others [16, 17] at high applied stress transitions to a *correlated* nucleation process. This transition is marked by a discontinuity in the activation energy versus stress, and a piecewise continuous shift in activation volume, and can be linked to the degree of metastability of the split-core structure. We focus in detail on α-Fe, but show that the effect is also observed in other potentials for BCC metals that predict the existence of the compact core structure.

2. Computational details

A $\frac{1}{2}\langle 1\,1\,1\rangle$ screw dislocation was setup in a simulation cell to study slip on the $\{1\,1\,0\}$ plane, in a geometry similar to that studied in previous studies [5, 31]. The defect-free crystal was oriented with $\vec{s}_1 = [\bar{1}\,0\,1]$, $\vec{s}_2 = [\bar{1}\,2\,\bar{1}]$, $\vec{s}_3 = [1\,1\,1]$, with periodic boundary conditions employed along the dislocation line and normal to the glide plane. Free surfaces were maintained in the direction of the dislocation motion. The screw dislocation was inserted into the simulation cell by Volterra shear, and relaxed with a conjugate gradient scheme to find the minimum energy core state. Most of our calculations have focused on α-Fe, for which we have employed the potential due to Mendelev [18]. Calculations for other BCC metals reported here have been performed using the potentials due to Ackland anf Thetford [15].

The dimensions of the simulation cell perpendicular to the dislocation line were approximately 100 Å $\times$ 100 Å, while the dislocation line length was varied. For examination of the 2D transition pathway, a narrow cut of $6b$ was used, where b is the Burgers vector. To study the 3D kink-nucleation process, dislocation lengths of 40, 80 and $120b$ were employed. The largest of these cells contain 252 000 atoms.

To setup a final state for the NEB transition pathway search, we loaded an incremental shear stress σ_{13} to the initial relaxed dislocation structure, with subsequent relaxation, until the dislocation jumped to the adjacent Peierls valley. The configuration was then unloaded and relaxed to a desired applied stress. Intermediate configurations for the NEB calculations were generated through linear interpolation in the 2D case, and in the 3D case, with constrained shifting of atomic rows within the dislocation core over a portion of the dislocation. Between 12 and 20 replicas were used to describe the path. All NEB calculations reported here were performed at constant stress, although constant volume simulations resulted in very similar results.

We employed differential displacement (DD) maps [32] and a central-symmetry parameter [33] masked threshold to identify and visualize the screw dislocation core and kink-pair structures, respectively. The latter was generated using AtomEye [34].

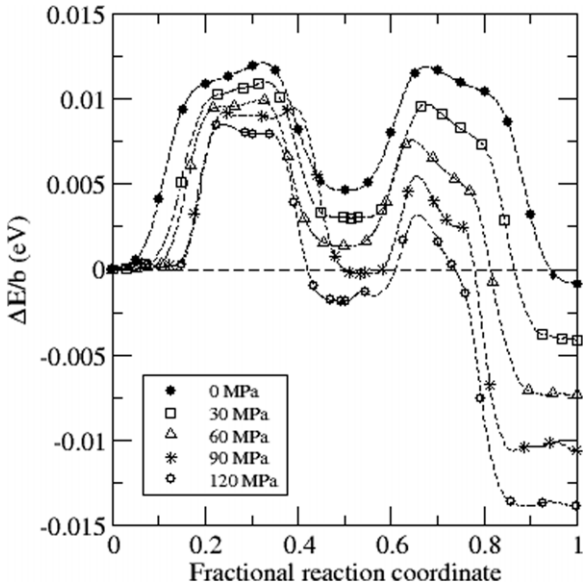

Figure 2. 2D minimum energy pathways for screw dislocation translation along the {1 1 0} glide plane using the Mendelev potential for Fe at various levels of applied shear stress.

3. Results and discussion

3.1. 2D Pathways

Before discussion of the full 3D kink-nucleation process, we first examine the 2D transition pathway, as this process is frequently studied to infer behavior in 3D. Figure 2 depicts the pathways in α-Fe plotted as a function of fractional reaction coordinate for applied shear stress ranging from 0–150 MPa. The energy per unit burgers vector is plotted relative to the initial state. At zero stress, the path follows the familiar camel-hump shape as the core transforms from the compact state to the split state (cf figures 1(*b*) and (*c*)). and back to the compact state in the next Peierls valley. At zero stress, the energy difference between the split core and compact core is approximately 0.0045 $\frac{\text{eV}}{b}$. With increasing stress, the work done on the system, $\sigma_{13}bd\theta$ [35], where d is the distance between Peierls valleys and θ is the fractional reaction coordinate, tilts the pathway, lowering both the transition barriers from compact $\Rightarrow$ split $\Rightarrow$ compact core. These results are in agreement with similar calculations reported in Rodney and Proville [35].

Increasing stress also lowers the relative energy difference between the split and compact core structures. This energy difference, $\Delta E_{\text{sc–cc}}$, is plotted in figure 3. Above a particular stress, the split-core structure, *with the aid of the applied stress*, becomes lower in energy than the initial compact core structure. We denote the stress at which the split-core structure becomes lower in energy than the compact ground state as σ_{th}, the *threshold* stress, and marks the zero in the ordinate of figure 3, which for the Mendelev Fe potential yields $\approx$85 MPa. This feature is key to understanding the 3D kink-nucleation process, as will be shown in the next section.

We also note that this characteristic is not unique to the Fe potential of Mendelev; we have performed similar calculations with Finnis–Sinclair-type potentials for Ta, V and Nb [15], all of which predict compact core structures [13]. The 2D transition pathways at zero stress

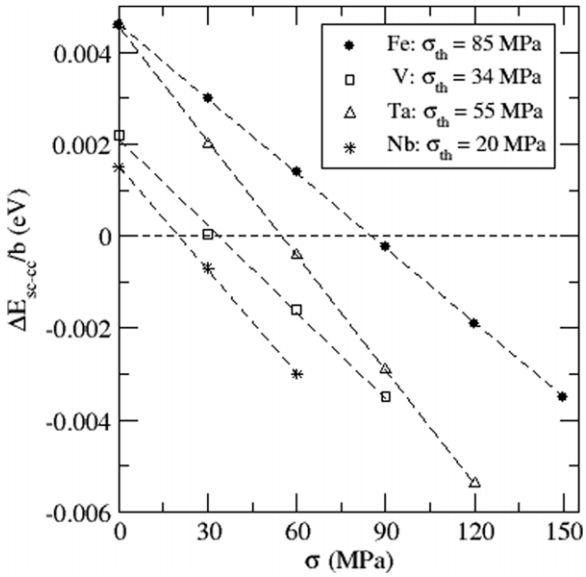

Figure 3. Energy difference between split and compact core structures versus applied shear stress for Fe, Nb, V and Ta. Threshold stress defined as the stress at which the energy difference is zero.

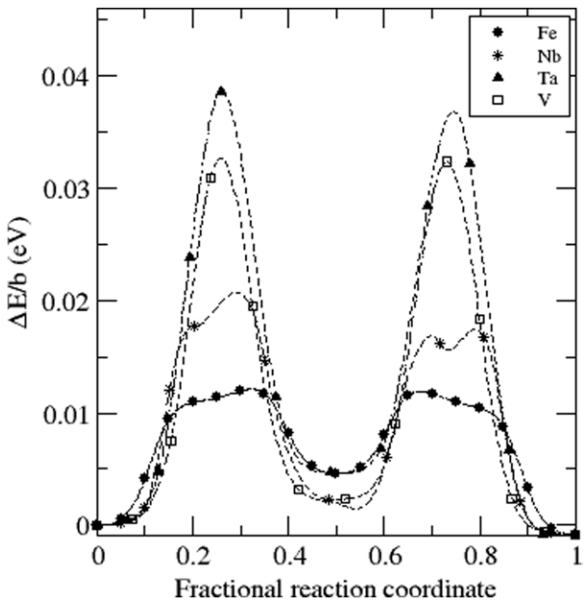

Figure 4. Comparison of 2D minimum energy pathways for screw core translation along the {1 1 0} glide plane at zero stress using potentials for Fe, Nb, V and Ta.

are plotted in figure 4, which all show a similar camel-hump shaped transition path, with an intermediate metastable split-core structure at the midpoint. Note that the depth of the metastable minimum in the path varies widely among the various potentials. The stress dependence of $\Delta E_{\mathrm{sc-cc}}$ for these models is also plotted in figure 3, from which the threshold stress can be identified as 55 MPa, 34 MPa and 20 MPa for Ta, V and Nb, respectively.

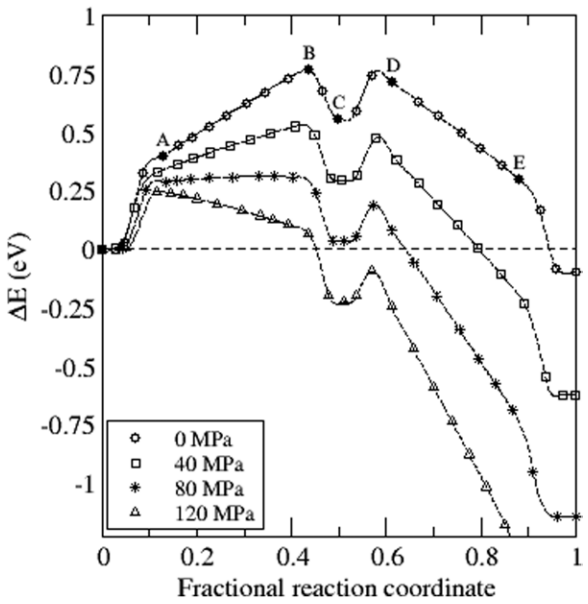

Figure 5. Transition pathways at various levels of applied stress for *uncorrelated* kink nucleation processes involved in screw dislocation motion.

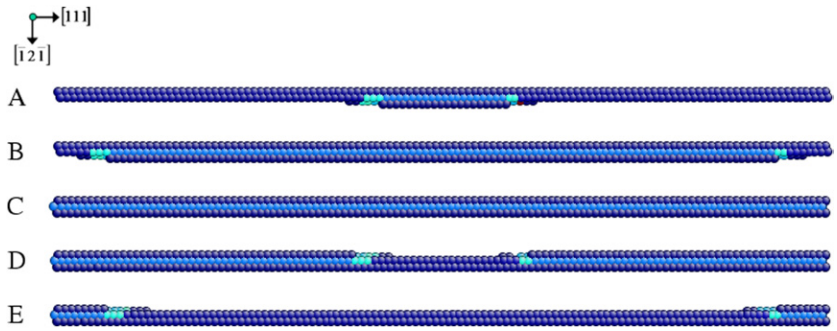

Figure 6. Snapshots of dislocation configurations along transition pathway corresponding to *uncorrelated* kink-nucleation processes at zero stress. Coloring of atoms corresponds to central symmetry parameter (green is high, blue is low). Labels A–E correspond to positions along path marked in figure 5. See text for additional details.

3.2. 3D pathways

As mentioned in the introduction, several authors have recently employed molecular dynamics to study screw dislocation motion with the Fe potential of Menedelev, and have noted that the motion occurs through two partial kink-pair processes. These studies were restricted to high applied stresses in order to induce motion in a reasonable timeframe. Here, we elucidate the pathways associated with these processes. In figure 5 we depict transition pathways of the screw dislocation at several different values of applied stress. Snapshots of configurations along the path labeled A–E are depicted in figure 6. The pathways depicted describe motion comprised of two partial kink-pair processes. First a *leading partial kink pair* is nucleated (image A) that transforms the compact core into the split core. The kinks continue to spread

along the line (image B) until they annihilate, leaving a full spit core structure (image C) in their wake. A *trailing partial kink pair* then nucleates (image D), transforming the split core to the compact core in the adjacent Peierls valley. The trailing kinks spread (image E) and finally annihilate, completing the dislocation motion.

The energy profiles associated with the transformation process described above indicate that the total energy expenditure can be viewed in terms of contributions arising from nucleating the leading kink pair, spreading the leading kink pair to produce the split-core structure and nucleation of the trailing kink pair. Of particular interest is the second of these contributions. At zero applied stress, the spreading of the kinks causes a linear increase in the system energy. For instance, the leading kink pair spreads approximately $0.7 \times 120b$ from image A to B, incurring a system energy increase of 0.37 eV. This agrees favorably with the 2D result, noting that at zero stress, we found that $\Delta E_{\text{sc–cc}} = 0.0045 \frac{\text{eV}}{b}$, and $84b \times \Delta E_{\text{sc–cc}}$ yields 0.38 eV. With increasing stress, the system energy increase becomes more gradual, as $\Delta E_{\text{sc–cc}}$ decreases. At 80 MPa, just below the previously identified *threshold stress*, σ_{th}, the spreading penalty has almost vanished. Well above σ_{th}, we can see that the work is sufficient to 'pay' for the transformation of the compact core to the split-core configuration.

Thus we see that the threshold stress separates the pathways described in figure 5 into two regimes. Below σ_{th}, the activation energy is dependent on the dislocation length, while above it, this length dependence vanishes. Above σ_{th}, the leading kink pair can nucleate and spread arbitrarily far prior to the nucleation of the trailing kink pair. We term this process the *uncorrelated* pathway because of this feature.

When we consider bulk single crystal or polycrystalline α-Fe, screw dislocation lengths are typically observed to be quite long. For well-annealed crystals as used experimentally to measure the Peierls stress, the dislocation density is typically $10^{12}\,\text{m}^{-2}$ leading to an average dislocation length between pinning points of about $1\,\mu$m. At low applied stress, the leading kink pair will need to spread a considerable distance before they can annihilate at kink sinks, requiring a large amount of energy. In the example presented above, for instance, the nucleation process over a $120b$ segment requires 50% of the total apparent activation energy of 0.76 eV[Note 3] to be expended in the process of kink spreading. In actuality, the screw segment lengths can be expected to be much longer than that. Therefore, in 'bulk' crystals, the uncorrelated pathway would appear to be quite unfavorable below the threshold stress, and another more favorable pathway must exist to accommodate screw dislocation motion.

The uncorrelated kink-pair nucleation processes in figure 5 are characterized by the two nucleation events proceeding independently of one another; namely, the trailing kink pair nucleates without the influence of the leading pair. At low applied stress, where kink spreading produces an energetically unfavorable split-core structure, it is possible to hypothesize a pathway that minimizes the amount of split core through a *correlated* nucleation process of the trailing kink pairs. We have obtained a converged transition state pathway that describes the concerted nucleation and spreading of the leading and trailing kink pairs, and is plotted at several values of stress below σ_{th} in figure 7. Snapshots of images along the path at zero stress A–E are shown in figure 8. In this pathway, we see the trailing kink pair (image B) nucleate immediately after nucleation of the leading kink pair (image A). The two kink pairs are separated by a short segment of split core, and the kinks spread out in a concerted fashion

[3] For simplicity, we assume the activation energy is the highest point on the curve; however, we note a non-trivial energy penalty of ≈0.2 eV at zero stress for nucleation of the trailing partial kink pair. This is somewhat lower than the apparent energy to nucleate the leading kink pair, and diminishes with increasing stress, so we assume that the activation energy will be given by the energy to nucleate the leading partial kink pair and, if below σ_{th}, the energy to spread the kinks.

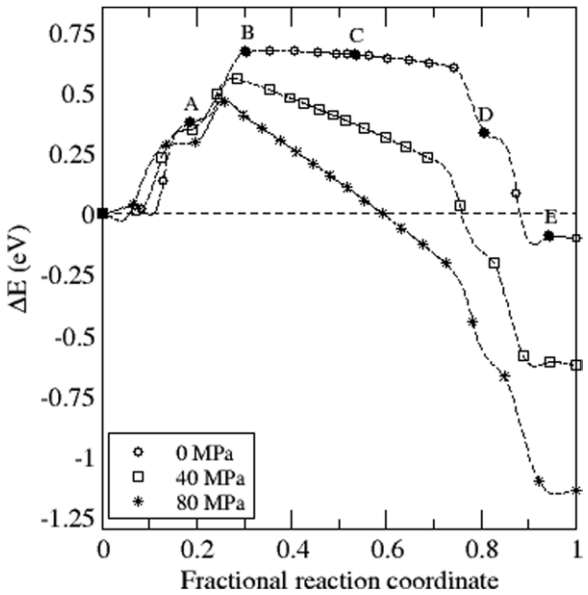

Figure 7. Transition pathways at various levels of applied stress for *correlated* kink-nucleation processes involved in screw dislocation motion.

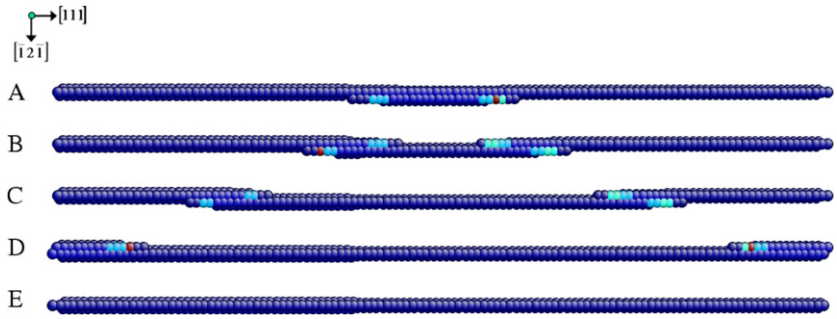

Figure 8. Snapshots of dislocation configurations along transition pathway corresponding to *correlated* kink-nucleation processes at zero stress. Labels A–E correspond to positions along path marked in figure 7. See text for additional details.

along the line (image C), which, at zero stress, produces a slight downward slope in the energy[4]. Annihilation proceeds with the leading (image D) and trailing kinks (image E) to return to the final compact core structure.

The snapshot of the 'full' kink structure, composed of a leading and trailing partial kink separated by a split-core segment, is reminiscent of two Shockley partial dislocations separated by a stacking fault in FCC crystals. One may speculate that by analogy, the length of the split-core segment separating the kink pairs will be inversely proportional to $\Delta E_{\mathrm{sc-cc}}$. The appealing feature of this *correlated* processes is that, below σ_{th}, the activation energy exhibits

[4] The slight negative slope of the energy profile at zero stress is caused by the translation of the screw dislocation toward one of the free surfaces in the simulation cell, where the imbalance in image forces results in a decrease in the system energy proportional to the length of the dislocation in the adjacent Peierls valley.

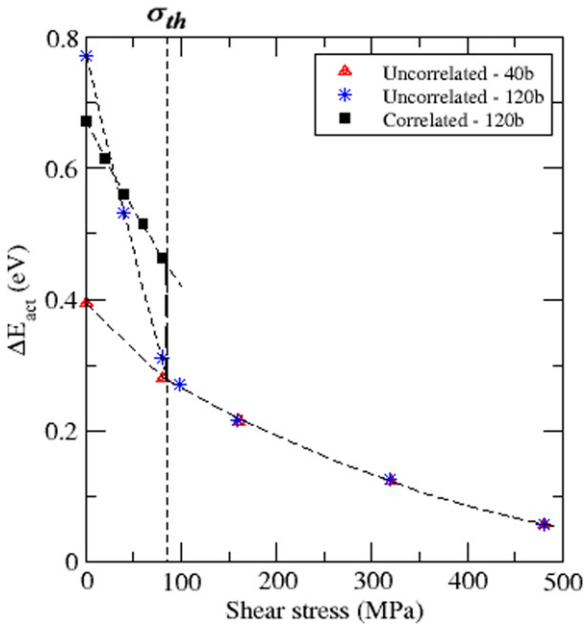

Figure 9. Activation energy for kink-pair nucleation for α-Fe as a function of applied stress for correlated and uncorrelated pathways. The threshold stress, $\sigma_{\rm th}$, is marked on the figure. Below the threshold stress, the uncorrelated pathway is dislocation length dependent.

no dependence on the length of the dislocation. The apparent activation energy now is easily estimated from the maximum in the curves of figure 7, which can be seen to be comprised of nucleation of the two partial kink pairs and a small segment of higher energy split core.

A comparison of the energetics associated with the correlated and uncorrelated pathways is shown in figure 9. Below the threshold stress, the uncorrelated pathway exhibits length dependence, and the activation energies computed for 40*b* and 120*b* dislocation lengths are plotted. As stated above, it seems likely that motion of long glissile dislocation segments would make the correlated pathway more favorable at low stress. However, above the threshold stress, the correlated pathway apparently becomes less favorable than the uncorrelated pathway, as attempts to compute the energetics of the correlated pathway above the threshold stress invariably resulted in convergence to the pathway corresponding to the uncorrelated process. This is due to the fact that part of the overall energetic cost associated with the correlated path includes the cost of nucleating the trailing kink pair, whereas in the uncorrelated path, the trailing kinks nucleate much later in the process. For the uncorrelated process, the energy required to nucleate the trailing kinks is lower than the leading kinks, and is presumed to be not rate-limiting for the overall motion of the screw dislocation. A similar discontinuity in the predicted kink formation energy versus stress has been observed in camel-hump Peierls potentials [36, 37], and the origin is presumed to be similar in this case.

We again note that this behavior is not restricted to the Fe potential of Mendelev *et al*. Figure 10 depicts the results for Ta, which exhibits qualitatively similar behavior, although the zero stress activation energy and the magnitude of the jump in apparent activation energy across the threshold stress are somewhat larger in this instance. This is consistent with the trend observed in the 2D pathways (figure 4), which shows that Ta has higher energetic barriers to overcome to reach the split-core structure, and the split core is situated in a deeper metastable

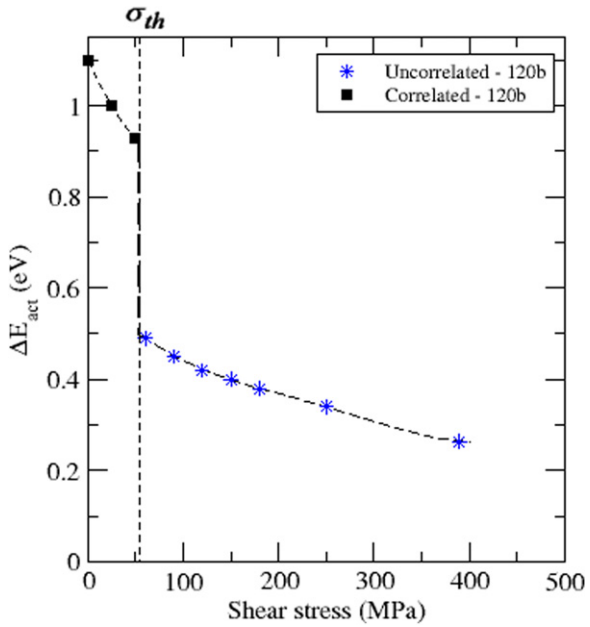

Figure 10. Activation energetics for kink-pair nucleation as a function of applied stress for correlated and uncorrelated pathways in Ta.

minimum. We conclude that the behavior exhibited by these potentials is a general consequence of the camel-hump shaped Peierls potential.

3.3. Comparison with Experiment

In figure 11 we compare the activation energy for kink-pair nucleation in α-Fe we have obtained in this work with experimental data [2, 11] and other simulation work reported in the literature [5]. Assuming an Arrhenius form to describe the thermally activated flow of dislocations, Aono *et al* showed that the exponential E/kT is nearly constant in the temperature range 30–340 K, with a value of 26 ± 1. This allows the flow stress versus temperature data to be recast in terms of activation energy versus stress, facilitating direct comparison with simulations that presume the flow stress is controlled by the kink-nucleation energetics. We observe excellent agreement with the experimental data up to the threshold stress. Above σ_{th}, the model clearly shows too small an activation volume, as indicated by $\frac{\mathrm{d}E_{\mathrm{act}}}{\mathrm{d}\sigma}$, as the activation energy falls off more slowly than the experimental data. Also plotted for comparison are the NEB calculations using a Johnson–Oh potential by Wen and Ngan. As noted in the introduction, this potential model predicts a degenerate core structure, and the most favorable kink-pair transition pathway found in their work is used for the comparison. Although the model predictions are reasonable at zero stress, it is clear that the results deviate significantly at higher stresses compared with experiment, and are in worse agreement than the model due to Mendelev. For instance, the zero-temperature flow stress (Peierls stress) is nearly three times greater than the experimental measurements. To explain the large discrepancy, it has been argued that in real crystals there must be sources of internal stress concentrations, such as from sessile dislocation pileups [38], that raise the applied stress to assist dislocation motion.

Another possible explanation for the overprediction of activation energies at elevated stress is that inertial effects play an increased role in the dynamics of the process. The argument here

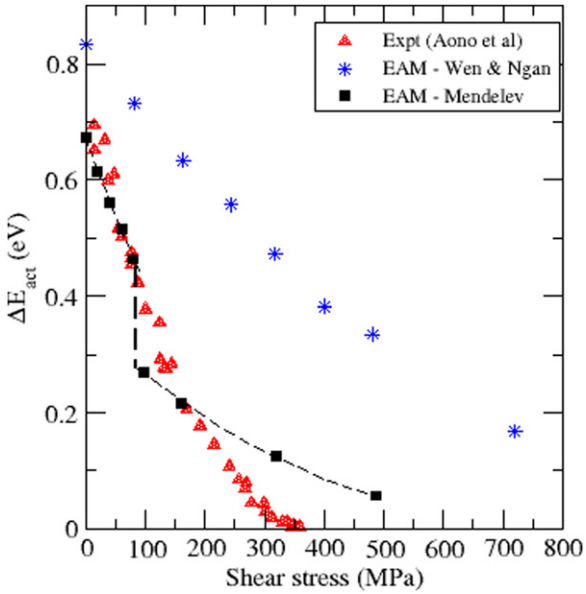

Figure 11. Comparison of activation energy versus shear stress for kink-pair nucleation in this work to other simulation work and experimental flow stress observations.

is that at elevated stress, the energetic barriers for kink nucleation are so reduced that a single nucleation event can trigger a series of subsequent nucleation events as the dislocation springs into motion [39]. Such an *avalanche* of events would lead to an increased traversal distance per nucleation event (or strain rate), and hence, a lower than expected activation energy for dislocation motion. Chaussidon *et al* [16] have attempted to characterize this directly using the same Fe potential employed in this work, by conducting molecular dynamics simulations of gliding screw dislocations over a range of elevated stresses and temperatures. They find that at stresses above 400–500 MPa, it is easy to observe multiple kink-pair nucleation events and at even higher stress, cross-slip, that suggest that classical transition state theory may not be appropriate to estimate the apparent activation energy of the screw dislocation motion. However, at lower applied stress, in the range 100–300 MPa, these inertial effects are not observed. This is somewhat disconcerting, since the Mendelev potential does not agree well with the experimental flow stress data in this region.

We have conducted similar molecular dynamics simulations to examine dynamics effects in the stress regime below 200 MPa, starting from the initial condition of a post-critical kink-pair nucleus ready to spread and move the dislocation into the next Peierls valley. We have found that the system will easily arrest in the split-core state, due to the relatively large metastable minimum in which the system finds itself. Relative to kT, the system appears to not have enough inertia to advance beyond the single nucleation event. This suggests that the transition state theory analysis should be appropriate in this regime, and the reason for disagreement with experiment may be due to inadequacies in the potential description.

4. Conclusions

In this work, we have explored the activated kink-nucleation process for interatomic potentials that predict a compact core structure and an intermediate, metastable split-core structure.

The ramifications of these structures, and the observation that, for many interatomic potentials, these structures go hand-in-hand, have been investigated in the context of the activation energies for kink nucleation as a function of applied stress. We find two active regimes, separated by a threshold stress, that govern the kink-nucleation process. At low stress, two correlated half-kink pairs are found to nucleate, whereas as higher stress, a second kink pair is found to nucleate independently after the first kink pair has spread along the dislocation line. This results in a discontinuity in the energetics describing the nucleation process, a necessary consequence of the potential.

In comparison with experimental data, the correlated nucleation mechanism for the Mendelev Fe EAM potential shows excellent agreement; this agreement diminishes above the threshold stress. This disagreement may be due to the potential description itself, which we will address in future work.

Acknowledgments

The authors gratefully acknowledge Mike Luton and Wei Cai for helpful discussions and suggestions throughout this work.

References

[1] Caillard D and Martin J-L 2003 *Thermally Activated Mechanisms in Crystal Plasticity* (Amsterdam: Elsevier) pp 85–122
[2] Suzuki T, Takeuchi S and Yoshinaga H 1991 *Dislocation Dynamics and Plasticity* (Berlin: Springer)
[3] Cai W, Chang J, Li J and Yip S 2004 Dislocation core effects on mobility *Dislocations in Solids* vol 12, ed J P Hirth (Amsterdam: Elsevier) pp 1–80 chapter 64
[4] Vitek V 1974 Theory of the core structures of dislocations in body-centered-cubic metals *Cryst. Latt. Defects* **5** 1–34
[5] Wen M and Ngan A H W 2000 Atomistic simulation of kink-pairs of screw dislocations in body-centered cubic iron *Acta Mater.* **48** 4255–65
[6] Ngan A H W and Wen M 2002 Atomistic simulation of energetics of motion of screw dislocations in bcc Fe at finite temperatures *Comput. Mater. Sci.* **23** 139–45
[7] Ngan A H W 2005 Non-planar dislocations: 3D models and thermally-activated glide processes *Mater. Sci. Eng.* A **400–401** 25–36
[8] Johnson R A and Oh D J 1989 Analytic embedded atom method for bcc metals *J. Mater. Res.* **4** 1195–201
[9] Duesbery M S 1983 On kinked screw dislocations in the b.c.c. lattice–I. The structure and peierls stress of isolated kinks *Acta Metall.* **31** 1747–58
[10] Duesbery M S 1983 On kinked screw dislocations in the b.c.c. lattice–II. kink energies and double kinks *Acta Metall.* **31** 1759–70
[11] Aono Y, Kuramoto E and Kitajima K 1981 Plastic deformation of high-purity iron single crystals *Rep. Res. Inst. Appl. Mech.* **XXIX** 127–93
[12] Takeuchi S 1979 Core structure of a screw dislocation in the B.C.C. lattice and its relation to slip behavior in α-iron *Phil. Mag.* A **39** 661–71
[13] Duesbery M S and Vitek V 1998 Plastic anisotropy in B.C.C. transition metals *Acta Mater.* **46** 1481–92
[14] Finnis M W and Sinclair J E 1984 A simple empiricdal N-body potential for transition metals *Phil. Mag.* A **50** 45–55
[15] Ackland G J and Thetford R 1987 An improved N-body semi-empirical model for body-centered cubic transition metals *Phil. Mag.* A **56** 15–30
[16] Chaussidon J, Fivel M and Rodney D 2006 The glide of screw dislocations in bcc Fe: atomistic static and dynamic simulations *Acta Mater.* **54** 3407–16
[17] Domain C and Monnet G 2005 Simulation of screw dislocation motion in iron by molecular dynamics simulations *Phys. Rev. Lett.* **95** 215506
[18] Mendelev M I, Han S, Srolovitz D J, Ackland G J, Sun D Y and Asta M 2003 Development of new interatomic potentials appropriate for crystalline and liquid iron *Phil. Mag.* **83** 3977–94

[19] Simonelli G, Pasianot R and Savino E J 1993 Embedded-atom-method interatomic potentials for bcc-Iron *Mater. Res. Soc. Symp. Proc.* **291** 567–72
[20] Ackland G J, Bacon D J, Calder A F and Harry T 1997 Computer simulation of point defect properties in dilute Fe–Cu alloy using a many-body interatomic potential *Phil. Mag.* A **75** 713–32
[21] Dudarev S L 2003 Coherent motion of interstitial defects in a crystalline material *Phil. Mag.* **83** 3577–97
[22] S Chiesa, Gilbert M R, Dudarev S L, Derlet P M and Van Swygenhoven H 2009 The non-degenerate core structure of a $1/2\langle 1\,1\,1\rangle$screw dislocation in bcc transition metals modelled using Finnis–Sinclair potentials: the necessary and sufficient conditions *Phil. Mag.* **89** 3235–43
[23] Ismail-Beigi S and Arias T A 2000 *Ab initio* study of screw dislocations in Mo and Ta: a new picture of plasticity in bcc transition metals *Phys. Rev. Lett.* **84** 1499–502
[24] Frederiksen S L and Jacobsen K W 2003 Density functional theory studies of screw dislocation core structures in bcc metals *Phil. Mag.* **83** 365–75
[25] Segall D E, Strachan A, Goddard W A, Ismail-Beigi S and Arias T A 2003 *Ab initio* and finite-temperature molecular dynamics studies of lattice resistance in tantalum *Phys. Rev.* B **68** 014104
[26] Ventelon L and Willaime F 2007 Core structure and peierls potential of screw dislocations in alpha-Fe from first principles: cluster versus dipole approaches *J. Comput.-Aided Mater. Des.* **14** 85–94
[27] Ventelon L and Willaime F 2010 Generalized stacking-faults and screw-dislocation core-structure in bcc iron: a comparison between ab initio calculations and empirical potentials *Phil. Mag.* **90** 1063–74
[28] Henkelman G and Jonsson H 2000 Improved tangent estimate in the nudged elastic band method for finding minimum energy paths and saddle points *J. Chem. Phys.* **113** 9978–85
[29] Henkelman G, Uberuaga B P and Jonsson H 2000 A climbing image nudged elastic band method for finding saddle points and minimum energy paths *J. Chem. Phys.* **113** 9901–4
[30] Henkelman G and Jonsson H 1999 A dimer method for finding saddle points on high dimensional potential surfaces using only first derivatives *J. Chem. Phys.* **111** 7010–22
[31] Rodney D 2007 Activation enthalpy for kink-pair nucleation on dislocations: comparison between static and dynamic atomic-scale simulations *Phys. Rev.* B **76** 144108
[32] Vitek V, Perrin R C and Bowen D K 1970 Core structure of $\frac{1}{2}\langle 1\,1\,1\rangle$ screw dislocations in bcc crystals *Phil. Mag.* **21** 1049–73
[33] Li J 2005 Atomistic visualization *Handbook of Materials Modeling* vol Pt A, ed S Yip (Berlin: Springer) pp 1051–68
[34] Atomeye J Li 2003 AtomEye: an efficient atomistic configuration viewer *Modelling Simul. Mater. Sci. Eng.* **11** 173–7
[35] Rodney D and Proville L 2009 Stress-dependent peierls potential: Influence on kink-pair activation *Phys. Rev.* B **79** 094108
[36] Guyot P and Dorn J E 1967 A critical review of the peierls mechnaism *Can. J. Phys.* **45** 983–1016
[37] Suzuki T, Koizumi H and Kirchner H O K 1995 Plastic flow stress of b.c.c. transition metals and the peierls potential *Acta Metall. Mater.* **43** 2177–87
[38] Groger R and Vitek V 2007 Explanation of the discrepancy between the measured and atomistically calculated yield stresses in body-centered cubic materials *Phil. Mag. Lett.* **87** 113–20
[39] Suzuki T and Koizumi H 1993 Inertial motion and multi-kink pair formation of dislocations on the peierls potential *Phil. Mag.* A **67** 1153–60